

H¹³CN-HN¹³C INTENSITY RATIO AS A TEMPERATURE INDICATOR OF INTERSTELLAR CLOUDS

A. G. Pazukhin,^{1,2,*} I. I. Zinchenko,^{1,2,**} E. A. Trofimova,^{1,***} and C. Henkel^{3,4,****}

¹*Federal Research Center Institute of Applied Physics RAS, Nizhny Novgorod, Russia*

²*Lobachevsky State University of Nizhny Novgorod, Nizhny Novgorod, Russia*

³*Max Planck Institute for Radio Astronomy, Bonn, Germany*

⁴*King Abdulaziz University, Jeddah, Saudi Arabia*

(Received September 02, 2022; Revised October 10, 2022; Accepted October 20, 2022)

With the 30-m IRAM radio telescope, we observed several massive star forming regions at wavelengths of 3-4 and 2 mm. The temperature of the gas in the sources was estimated from the lines of CH₃CCH and from the transitions of the NH₃ molecule obtained during observations at the 100-m radio telescope in Effelsberg. As a result, a correlation between the integrated intensity ratios of the $J = 1 - 0$ transitions of H¹³CN and HN¹³C and the kinetic temperature has been obtained. The obtained results allow us to propose the use of the intensity ratio H¹³CN-HN¹³C as a possible temperature indicator of interstellar clouds. We also compared the obtained estimates of the kinetic temperature with the dust temperature T_{dust} . As a result, no significant correlation was found.

Keywords: star formation, interstellar medium, molecular clouds, temperature.

1. INTRODUCTION

The hydrogen cyanide molecule HCN and its isomer HNC are widely distributed in the interstellar medium. It is known that the HCN/HNC abundance ratio strongly depends on the kinetic temperature, for example, it was found in [1] that the abundance ratio in high

* Electronic address: pazukhinandrey@bk.ru

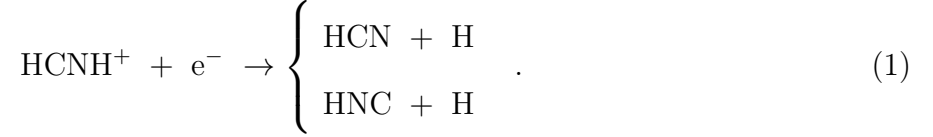
** Electronic address: zin@ipfran.ru

*** Electronic address: tea@ipfran.ru

**** Electronic address: chenkel@mpifr-bonn.mpg.de

mass protostellar objects is 4, in hot ultracompact H II regions the average value is 9. In [2] it was proposed to use the intensity ratio of HCN to HNC line as a temperature indicator based on observations of the integral shaped filament in Orion.

The main pathway for the formation of HCN and HNC isomers is the dissociative recombination of the HCNH^+ ion with an electron:



This reaction has an approximately equal branching ratio [3], and the abundance differences between HCN and HNC are largely determined by the destruction and isomerization reactions of HNC. These include the following reactions (e.g. [4]):



The energy barrier for the reaction (2) is 200 K [4], for the reaction (3) it is 20 K, which determines the dominant role of reaction (3) at low temperatures of the order of 50 K [2]. However, the classical calculated energy barriers are 1200 K and 2000 K, respectively (see details in [4]).

2. OBSERVATIONS AND DATA REDUCTION

2.1. *Observations at the 30-m radio telescope of the Institute of Millimeter Radio Astronomy (IRAM)*

In September 2019, with the 30-m radio telescope of the Institute of Millimeter Radio Astronomy (IRAM), we observed several massive star forming regions at wavelengths of 2 and 3–4 mm (as part of project 041-19). The list of sources is given in Table 1. In this paper, a part of the obtained data is discussed. Table 2 contains the corresponding list of molecular lines. The transition frequency and upper level energy are taken from the CDMS¹ catalogue.

¹ <http://cdms.de>

Table 1. List of sources

Object	α (2000)	δ (2000)	V_{lsr} km s ⁻¹	d kpc	Note
L 1287	00 ^h 36 ^m 47.5 ^s	63°29′02.1″	-17.7	0.93	G121.30+0.66, IRAS 00338+6312
S 187	01 23 15.4	61 49 43.1	-14.0	1.0	G126.68-0.81, IRAS 01202+6133
S 231	05 39 12.9	35 45 54.0	-16.6	2.3	G173.48+2.45, IRAS 05358+3543
DR 21(OH)	20 39 00.6	42 22 48.9	-03.8	1.5	G81.72+0.57
NGC 7538	23 13 44.7	61 28 09.7	-57.6	2.8	G111.54+0.78, IRAS 23116+6111

Note. Distances to sources are quoted from [5–7]

The full beam width at half maximum at the discussed frequencies ranged from $\sim 30''$ to $\sim 16''$. The antenna temperature T_A^* was reduced to the main beam temperature T_{mb} , using the main beam efficiency B_{eff} , which was determined by the Ruze’s equation in accordance with the IRAM recommendations and ranged from 0.72 to 0.82. The minimum system noise temperature was ~ 100 K in the 3 mm range and ~ 200 K in the 2 mm range.

Observations were carried out by the method of continuous mapping (OTF, On-The-Fly) of a $200'' \times 200''$ area in full power mode. The reference position was chosen with a shift of $10'$ in right ascension. In some extended sources, i.e. DR 21(OH) and NGC 7538, two partially overlapping areas were observed. The pointing accuracy was checked periodically by observations of nearby continuum sources.

2.2. Observations at the Max-Planck-Institute for Radio Astronomy with the Effelsberg 100-m radio telescope

On 9 December 2019 we observed with the 100-m telescope near Effelsberg (Germany) the H₂O maser transition at a frequency of 22 GHz, as well as the ammonia inversion lines $(J, K) = (1,1)$, $(2,2)$ and $(3,3)$. The full beam width at half maximum was $\sim 40''$. The measurements were carried out by the method of continuous mapping using a K -band receiver in a secondary focus with a dual bandwidth of 300 MHz, including the aforementioned H₂O lines in one band and NH₃ in the other band. $5' \times 5'$ maps were obtained at a scanning rate of $20''$ per second in right ascension; intervals between scans were $15''$. The reference

Table 2. Observed molecular lines

Molecule	Transition	Frequency, MHz	E_u/k , K
NH ₃	(1, 1)	23694.495	23.4
	(2, 2)	23722.634	64.9
CH ₃ CCH	5 ₃ – 4 ₃	85442.601	77.3
	5 ₂ – 4 ₂	85450.766	41.2
	5 ₁ – 4 ₁	85455.667	19.5
	5 ₀ – 4 ₀	85457.300	12.3
H ¹³ CN	1 – 0	86339.921	4.1
HN ¹³ C	1 – 0	87090.825	4.2
HCN	1 – 0	88631.602	4.3
HNC	1 – 0	90663.568	4.4
CH ₃ CCH	9 ₃ – 8 ₃	153790.772	101.9
	9 ₂ – 8 ₂	153805.461	65.8
	9 ₁ – 8 ₁	153814.276	44.1
	9 ₀ – 8 ₀	153817.215	36.9

position was shifted by +15' in azimuth. Weather conditions included light rain with low wind speeds ($\sim 2 \text{ m s}^{-1}$).

The source NGC 7027 was used for calibration with a flux density of 5.5 Jy at 22 GHz [8]. The antenna temperature T_A^* was obtained by multiplying the observed intensities by T_{cal} and taking into account atmospheric absorption².

2.3. Data reduction

The GILDAS/CLASS software³ was used for data reduction. The IRAM-30m and Effelsberg-100m datasets were reduced to the same spatial resolution of 40". After baseline subtraction and smoothing, the spectral resolution for the Effelsberg-100m data was $\sim 0.46 \text{ km s}^{-1}$.

² <http://eff100mwiki.mpifr-bonn.mpg.de>

³ <http://www.iram.fr/IRAMFR/GILDAS>

In the analysis, integrated intensity maps ($I = \int T_{mb} dV$ in units $\text{K} \cdot \text{km s}^{-1}$) were used in the velocity range $[V_{lsr}-10, V_{lsr}+10]$ for HCN, H^{13}CN and $[V_{lsr}-4, V_{lsr}+4]$ for HNC, HN^{13}C . It should be noted that two velocity components ~ -4 and $\sim 0 \text{ km s}^{-1}$ are observed in the source DR 21(OH) (see details in [9]). In the reduction, the components were separated, and only the $\sim -4 \text{ km s}^{-1}$ component has been used for the analysis, since it is stronger and is detected throughout the source.

3. RESULTS

3.1. Kinetic temperature from observations of CH_3CCH

In [10, 11] it was shown that the rotational temperature of CH_3CCH gives a good estimate of the gas kinetic temperature at gas density $n \gtrsim 10^{3-4} \text{ cm}^{-3}$ (transitions $J = 5 - 4$ and $J = 6 - 5$ were considered). It is explained by the fact that, due to the low dipole moment ($\mu = 0.78 \text{ D}$), the CH_3CCH molecule is easily thermalized under such conditions. Gas density in our sources are above this threshold (Pazukhin et al., in preparation). Thus, the CH_3CCH lines in our data can be a good gas kinetic temperature indicator. Rotational (and, accordingly, kinetic) temperature is determined by the population diagrams method:

$$\ln \left(\frac{3k \int T_{mb} dv}{8\pi^3 \nu \mu^2 g_I g_K S} \right) = -\frac{E_u}{T_{kin}} + \ln \left(\frac{N_{tot}}{Q} \right), \quad (4)$$

where S is the line strength equal to $\frac{J^2-K^2}{J}$, ν is the transition frequency, E_u is the upper energy level in temperature units, μ is the dipole moment, $\int T_{mb} dv$ is the integrated line intensity, N_{tot} is the total column density, Q is the partition function, g_K is the K degeneracy associated with the internal quantum number K due to the projection of the total angular momentum onto a molecule axis, g_I is the statistical weight associated with the nuclear spin. It is assumed here that the emission is optically thin and the background radiation can be neglected.

The rotational diagrams were constructed using the $J = 5 - 4$ and $J = 9 - 8$ transitions of the CH_3CCH molecule. The spectra were fitted with Gaussian profiles, assuming that the widths of each component are equal, and the spacings between them are known. Then a graph was built, where the upper energy level E_u was plotted along the abscissa axis, and the left part of the equation (4) was plotted along the ordinate axis. Then, T_{kin} is proportional to the inverse of the slope. In Figure 1 in the direction IRAS 23116+6111 and DR 21(OH) the

spectra of the CH_3CCH molecule and rotational diagrams are plotted. Figure 2(left) shows a comparison of the kinetic temperature estimates for the $J = 5 - 4$ and $J = 9 - 8$ CH_3CCH transitions. In general these estimates are close to each other, therefore, the population diagram can be plotted using both transitions.

It should be noted that for the L 1287, estimates of the kinetic temperature were obtained only at two positions ($0''$, $0''$) and ($-14''$, $-14''$) and are equal to 21.5 ± 1.9 K and 20.4 ± 1.8 K, respectively. For S 187, S 231, the CH_3CCH lines turned out to be too weak to estimate the kinetic temperature.

3.2. Kinetic temperature from NH_3 observations

Transitions of the NH_3 molecule were observed in the sources S 187, DR 21(OH) with the Effelsberg-100m radio telescope. For S 231, we used the estimate of the kinetic temperature with ammonia from [12].

The optical depth and rotational temperature were determined using the methods described in [13]. The spectra were fitted with Gaussian profiles, in the transition (1,1) the widths of each component were assumed to be equal, and the spacings between them are known. Assuming that hyperfine components are under LTE conditions, the optical depth $\tau(1, 1, m)$ can be determined from the ratio of the main and satellite line intensities:

$$\frac{T_A^*(m)}{T_A^*(s)} = \frac{1 - \exp(-\tau(1, 1, m))}{1 - \exp(-a\tau(1, 1, m))}, \quad (5)$$

where T_A^* is the antenna temperature, a is the ratio of the main and satellite line intensities, equal to $a = 0.28$ for inner satellites and $a = 0.22$ for outer satellites. The optical depth $\tau(1, 1, m)$ was determined numerically from equation (5).

Thus, the rotational temperature can be obtained from the ratio of the main component intensities of (1,1) and (2,2) transitions using the equation:

$$T_{rot} = -41.5 \left/ \ln \left[\frac{-0.282}{\tau(1, 1, m)} \ln \left(1 - \frac{T_A^*(2, 2, m)}{T_A^*(1, 1, m)} \{1 - \exp(-\tau(1, 1, m))\} \right) \right] \right. \quad (6)$$

The kinetic temperature values were obtained using the equation from [14]:

$$T_{kin} = \frac{T_{rot}}{1 - \frac{T_{rot}}{41.5} \ln \left[1 + 1.1 \exp \left(-\frac{16}{T_{rot}} \right) \right]}. \quad (7)$$

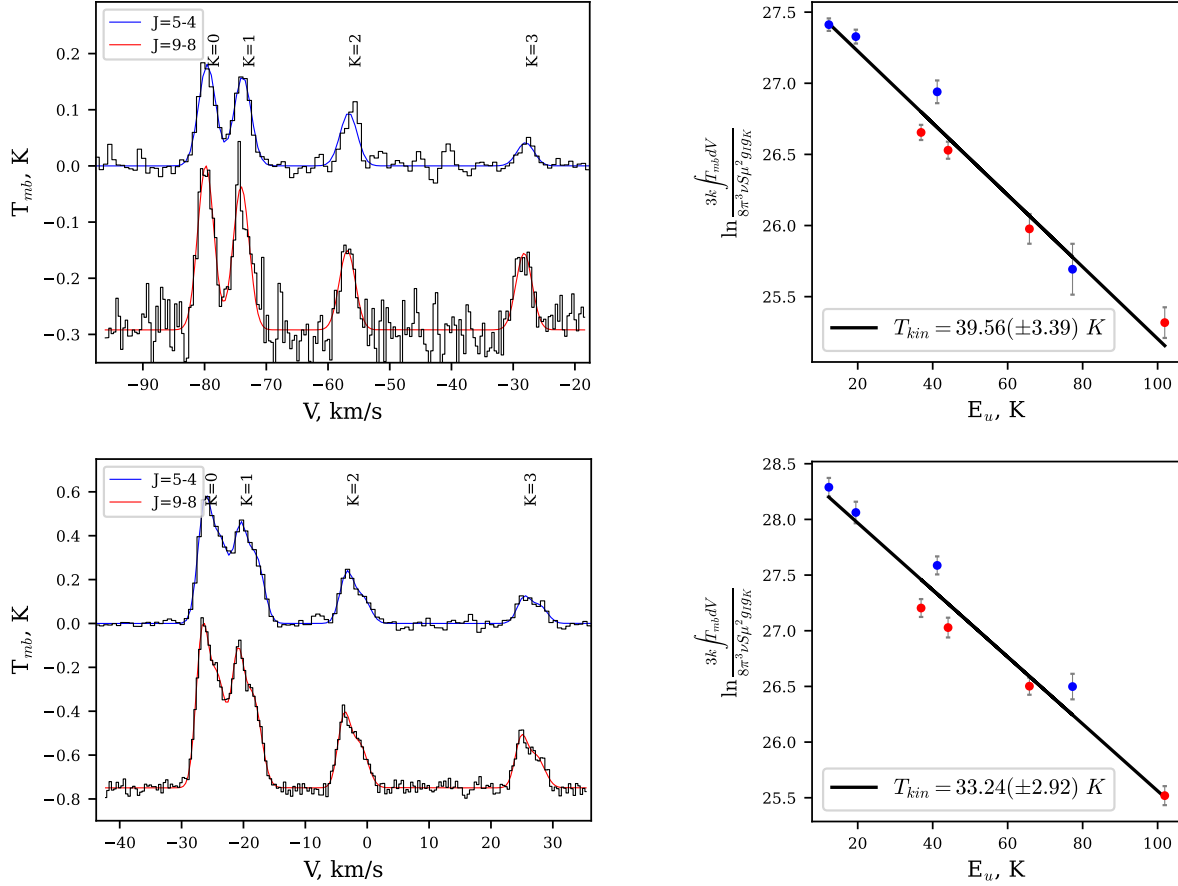


Figure 1. Spectra (left) and population diagrams (right) for IRAS 23116+6111 (upper panels) and DR 21(OH) (lower panels). CH₃CCH $J = 9 - 8$ and $J = 5 - 4$ spectra are indicated in black; the red and blue lines are the Gaussian profile fitting. The lines in the population diagrams are plotted by the least squares method. In the lower left corner of the diagrams, the obtained value of the kinetic temperature is given. For DR 21(OH), the Gaussian profiles are plotted for the velocity components ~ -4 and ~ 0 km s⁻¹, and the population diagram are plotted for the ~ -4 km s⁻¹ component.

4. DISCUSSION

Figure 2(right) shows a comparison of the kinetic temperature estimates from ammonia and CH₃CCH transitions for the DR 21(OH) source. In general, there is a fairly good agreement between them, although the estimates for the CH₃CCH transitions result in slightly higher values than the estimates for ammonia. This is probably due to the fact that methylacetylene is observed in a denser gas, where the temperature is higher.

In addition, for the sources L 1287, DR 21(OH) and NGC 7538, there are maps of dust

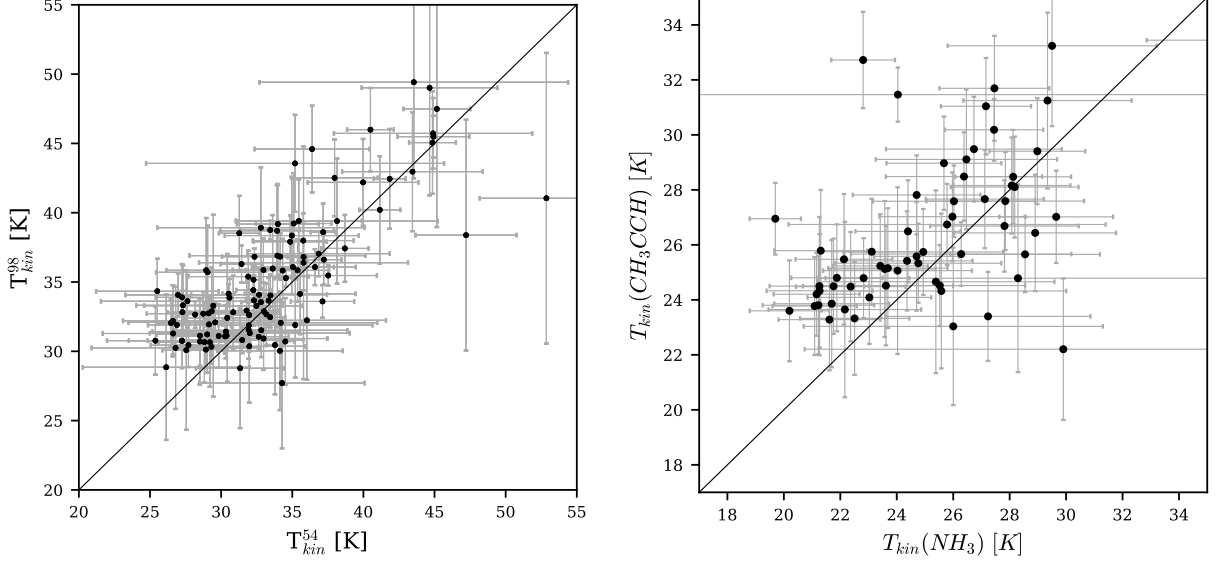


Figure 2. Comparison of estimates of the kinetic temperature from $J = 9 - 8$ and $J = 5 - 4$ CH_3CCH transitions (left) and for the source DR 21(OH) from ammonia and CH_3CCH transitions (right). Lines of the form $y = x$ are plotted diagonally.

temperature T_{dust} and column density $N(\text{H}_2)$ according to data from the Herschel telescope taken from the open database⁴, which were obtained using the PPMAP [15, 16] algorithm. We compared the dust temperature T_{dust} estimates with the kinetic temperature estimates (Fig. 3). As a result, no significant correlation was found. T_{dust} values are in the range $\sim 18 - 25$ K, while T_{kin} increase to 35 K. It is possible that the lack of correlation is due to the insufficient density of our sources. Thus, in [17] it is shown that the dust temperature approaches the gas temperature at a gas density $n \gtrsim 10^{7-8} \text{ cm}^{-3}$, which is much higher than the gas density estimates in our sources, which, according to our data, is $n \sim 10^{4-6} \text{ cm}^{-3}$ (Pazukhin et al., in preparation).

We estimated the optical depths in the HCN and HNC lines. To do this, we used the intensity ratio of the isotopologues $\text{HCN}/\text{H}^{13}\text{CN}$ and $\text{HNC}/\text{HN}^{13}\text{C}$ in the equation (5) and the value a from the abundance ratio of carbon isotopes [18]

$$\frac{^{12}\text{C}}{^{13}\text{C}} = 4.7 \times R_{GC} + 25.05,$$

where R_{GC} is the Galactocentric distance of the source. Figure 4(left) shows a comparison of the obtained optical depth values. The optical depths in both lines are large. The optical

⁴ <http://www.astro.cardiff.ac.uk/research/ViaLactea>

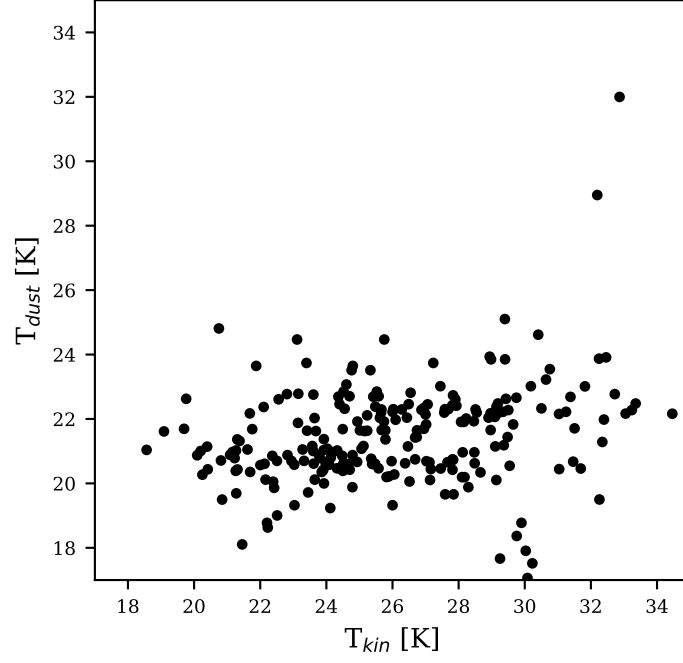


Figure 3. Comparison of dust temperature and kinetic temperature.

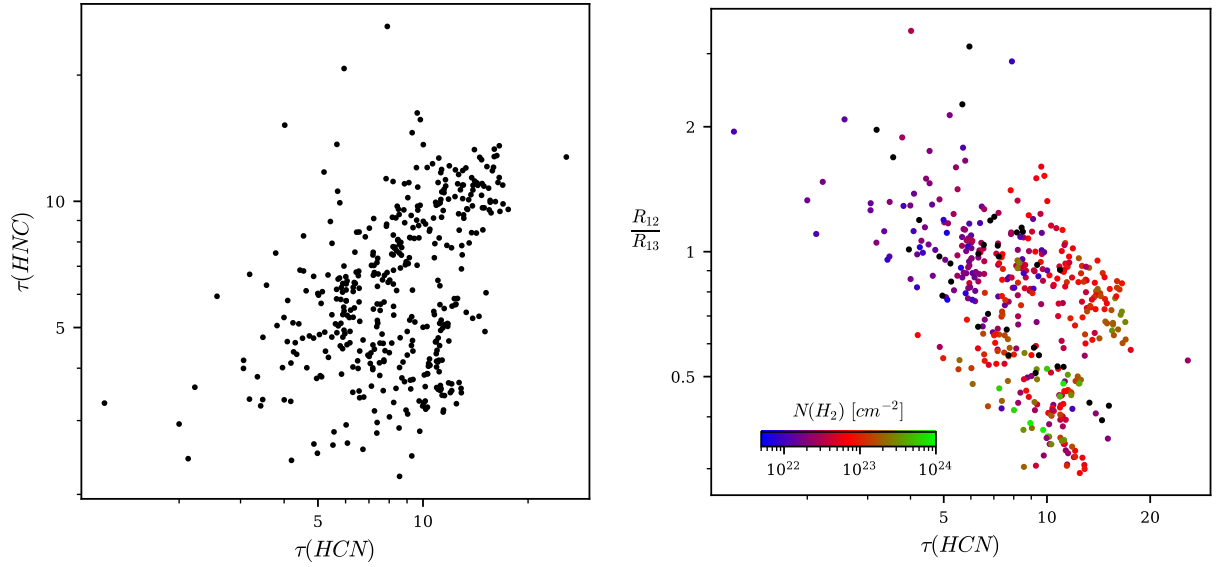


Figure 4. Dependence on the optical depth estimates $\tau(HCN)$ for HCN and HNC molecules of the $\tau(HNC)$ (left) and of the ratio R_{12}/R_{13} (right). The color code indicates to the column density $N(H_2)$ values.

depth in the HCN line is on average higher than in the HNC line and reaches ~ 20 . In this case, a rather large spread in the ratio of optical depths in these lines is observed. This makes it preferable to use the lines of their rare isotopologues H^{13}CN and HN^{13}C , in which the optical depth is obviously small. In [2] it was came to the conclusion that the optical depth in the HCN and HNC lines does not significantly affect the relation between the intensity ratio of these lines and the gas temperature. Our data cast doubt on this. Figure 4(right) shows the dependence of the ratio R_{12}/R_{13} [$R_{12} = I(\text{HCN})/I(\text{HNC})$ and $R_{13} = I(\text{H}^{13}\text{CN})/I(\text{HN}^{13}\text{C})$] on the optical depth $\tau(\text{HCN})$, as well as the values of the column density $N(\text{H}_2)$. It can be seen that at large optical depths, which are typical for HCN lines, the ratio R_{12}/R_{13} is much lower than unity. As the optical depth decreases, this ratio, as expected, tends to 1. The hydrogen column density, at which the optical depth in the lines becomes small, is $N(\text{H}_2) \sim 10^{22} \text{ cm}^{-2}$.

Variations of the R_{12} ratio can be caused by different excitation temperatures T_{ex} of HCN and HNC. However, on the dependence between T_{kin} and R_{12} plotted using the RADEX [19] program under the conditions $n = 10^5 \text{ cm}^{-3}$ and $N = 10^{12} \text{ cm}^{-2}$ it can be seen that the ratio changes only slightly with increasing temperature and amounts to $\lesssim 1$ (Fig. 5).

As a result of the analysis of our data, the dependence of the ratios R_{12} and R_{13} on the gas kinetic temperature was plotted (Fig. 6). The value of R_{13} increases from 1 to 10, and the intensity ratio of the main isotopologues increase from 1 to 4 in the temperature range $\sim 15 - 45 \text{ K}$.

Thus, as a result of the linear least squares fit, the following dependencies were obtained:

$$T_{kin} = \begin{cases} 2.4 \times R_{13} + 19.1, \\ 8.7 \times R_{12} + 6.4. \end{cases} \quad (8)$$

The line obtained for HCN and HNC agrees with the line $T_{kin} = 10 \frac{I(\text{HCN})}{I(\text{HNC})}$ obtained in [2], which is valid for intensity ratios ≤ 4 and up to temperatures $T_{kin} \sim 40 \text{ K}$.

In addition, Figure 6 shows an approximation by a function of the form $A \exp\left(\frac{-\Delta E}{T_{kin}}\right)$, which is chosen based on the population ratio expressed in terms of the Boltzmann distribution. As a result, the following dependencies were:

$$R_{13} = 179 \times \exp\left(\frac{-109}{T_{kin}}\right), \quad (9a)$$

$$R_{12} = 8.4 \times \exp\left(\frac{-34}{T_{kin}}\right). \quad (9b)$$

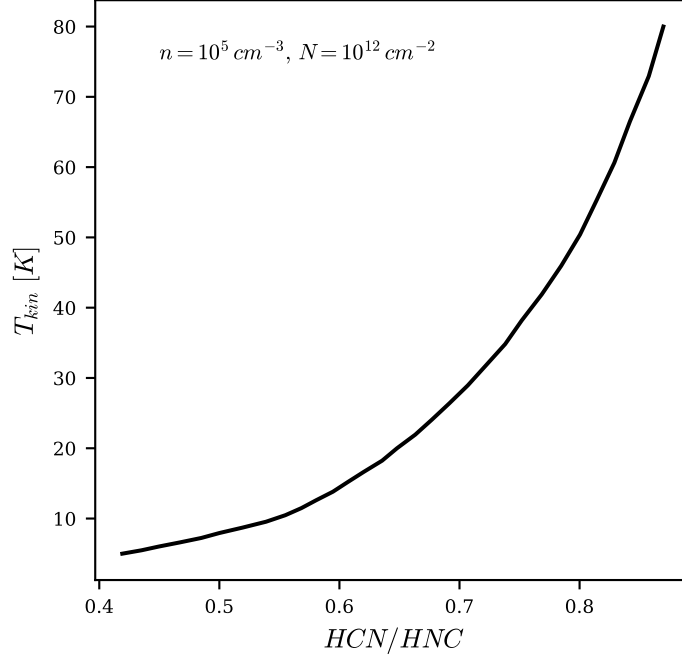


Figure 5. Dependence of the kinetic temperature T_{kin} on the ratio R_{12} plotted using the RADEX program for $n = 10^5 \text{ cm}^{-3}$ and $N = 10^{12} \text{ cm}^{-2}$.

The energy barrier for the ratio R_{13} is $\Delta E \sim 109 \text{ K}$, and for the main isotopologues is $\Delta E \sim 34 \text{ K}$. The results from other publications are somewhat different, the energy barrier at low temperatures is $\Delta E \sim 20 \text{ K}$ [2], with a further increase with temperature $\Delta E \sim 200 \text{ K}$ [4, 20].

In general, the data for HCN and HNC agree with the results from [2]. However, the results for R_{13} are noticeably different. The main reason for the discrepancy between the results is probably the large optical depth of the HCN and HNC lines, as well as the presence of anomalies in the hyperfine structure of the HCN molecule.

The use of the H^{13}CN and HN^{13}C lines for temperature estimation was also recently proposed and demonstrated in [21]. However, in this paper, to estimate the temperature, the correlation dependence of R_{12} on temperature found in [2] is used. As shown above, the dependence of R_{13} on temperature differs from it.

We suppose that it is preferable to use the equation (9a) for the ratio R_{13} as a temperature indicator. Temperature estimates for NGC 7538 and DR 21(OH) are shown in Figure 7. The plotted maps demonstrate good agreement with the estimates obtained from the CH_3CCH and NH_3 lines. The temperature gradient is visible, the peaks spatially coincide with the

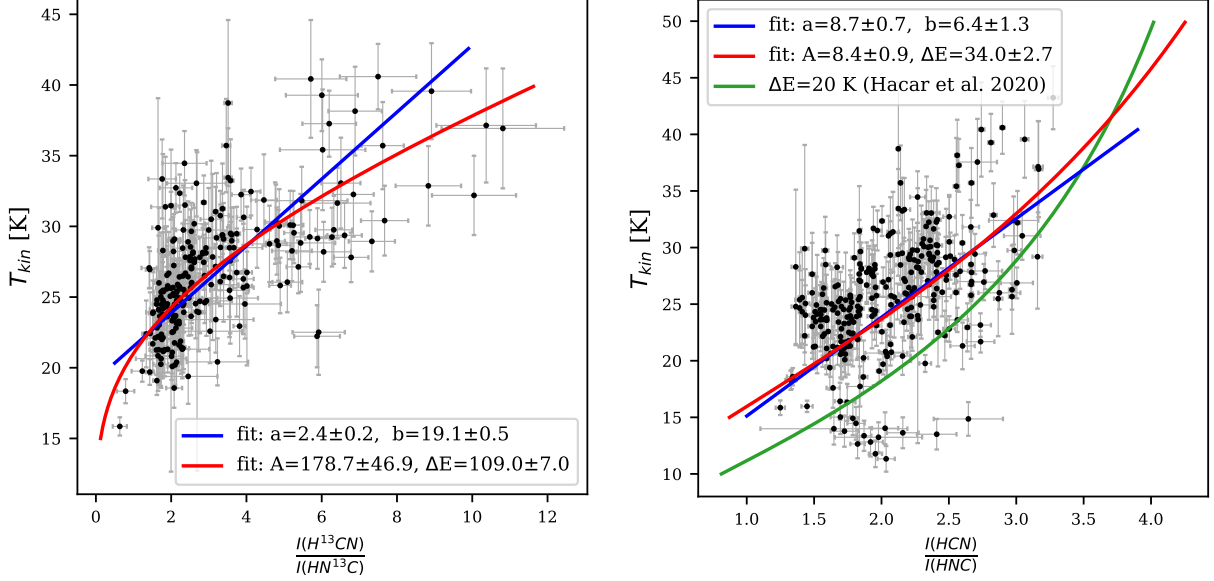


Figure 6. Dependence of the kinetic temperature on the integrated intensity ratio of the molecules H^{13}CN and HN^{13}C (left) and HCN and HNC (right). The fitting results are represented by the blue straight line $ax + b$ and the red curve describes a function $A \exp\left(\frac{-\Delta E}{T_{kin}}\right)$. The green curve corresponds to $\Delta E = 20$ K from [2]. The parameters of the fits (a , b , A , ΔE) are shown in each of the figures.

emission of the continuum and the emission of the IR source. In addition, maps are more extended than than plotted temperature maps obtained from lines of CH_3CCH and NH_3 .

It is worth noting that temperature maps can be further expanded by combining the observational data from isotopologues H^{13}CN and HN^{13}C with observations from the main isotopologues, for example, as suggested in [21]. In this paper, in those source regions where the H^{13}CN and HN^{13}C lines become too weak, the intensity ratio of the main isotopologues R_{12} is used.

5. CONCLUSION

Based on observations of five massive star-forming regions obtained with the IRAM-30m and Effelsberg-100m radio telescopes, as well as using estimates of the dust temperature T_{dust} from the Herschel telescope data, we obtained following results:

1. A correlation between the integrated intensity ratios of the $J = 1 - 0$ transitions of H^{13}CN and HN^{13}C and the kinetic temperature has been found. The intensity ratio

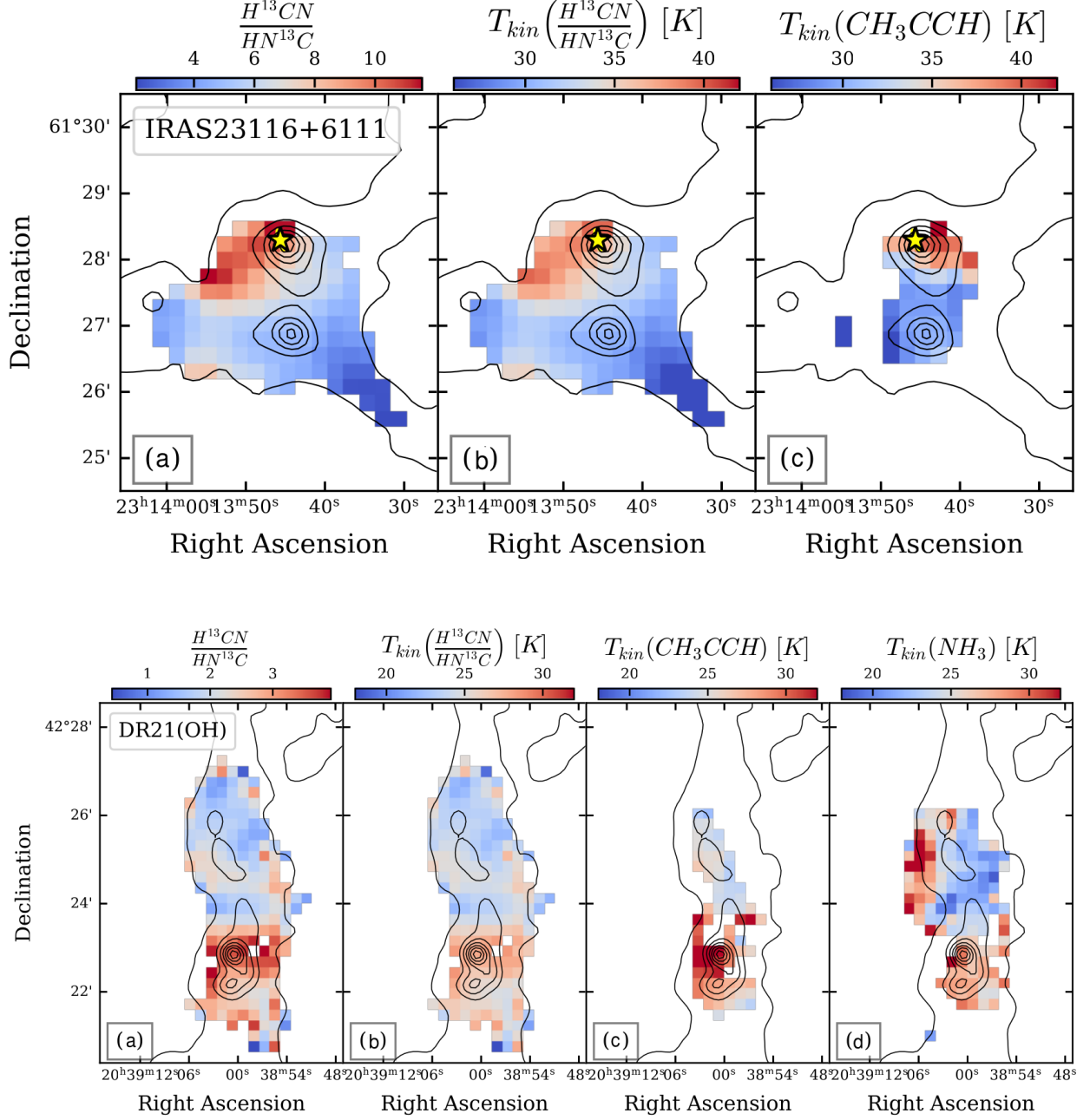


Figure 7. Maps for NGC 7538 (upper panels) and DR 21(OH) (lower panels). The integrated intensity ratio of the molecules $H^{13}CN$ and $HN^{13}C$ (a); $T_{kin}(H^{13}CN/HN^{13}C)$ (b), the kinetic temperature derived using CH_3CCH transitions (c) and the kinetic temperature derived using NH_3 transitions (d). The SCUBA 850 μm continuum data [22] are indicated by contours. The star-shaped marker indicates the IRAS 23116+6111 position.

increases from 1 to 10 in the temperature range $\sim 15 - 45$ K. Since these lines can be detected in observations of most sources, the results obtained allow us to propose using the intensity ratio $\text{H}^{13}\text{CN}/\text{HN}^{13}\text{C}$ as a possible temperature indicator of interstellar clouds.

2. For the low-temperature reaction $\text{HNC} + \text{O} \rightarrow \text{CO} + \text{NH}$, the energy barrier obtained from the ratio $\text{H}^{13}\text{CN}/\text{HN}^{13}\text{C}$ was $\Delta E \sim 109$ K, and from the ratio of the main isotopologues $\Delta E \sim 34$ K. The main reason for the discrepancy between the results is probably the large optical depth of the HCN and HNC lines, as well as the presence of anomalies in the hyperfine structure of the HCN molecule.
3. We compared the obtained estimates of the kinetic temperature with the estimates of the dust temperature T_{dust} . As a result, no significant correlation was found. T_{dust} values are in the range $\sim 18 - 25$ K, while T_{kin} grows up to 35 K. It is possible that the lack of correlation is due to the insufficient density of the observed sources.

FUNDING

The research was supported by the Russian Science Foundation (grant no. 22-22-00809).

ACKNOWLEDGMENTS

The research is based on observations made by the 041-19 project with the 30-m telescope, as well as observations with the 100-m MPIfR telescope (Max-Planck-Institut für Radioastronomie) in Effelsberg. IRAM is supported by INSU/CNRS (France), MPG (Germany) and IGN (Spain). We acknowledge the staff of both observatories for their support in the observations. The authors are grateful to the anonymous reviewer for useful comments that improved the quality of the paper.

-
1. M. Jin, J.-E. Lee, and K.-T. Kim, *Astrophys. J. Suppl. Ser* **219**, 2 (2015), 1505.00849.
 2. A. Hacar, A. D. Bosman, and E. F. van Dishoeck, *Astron. Astrophys* **635**, A4 (2020), 1910.13754.

3. M. B. Mendes, H. Buhr, M. H. Berg, M. Froese, M. Grieser, O. Heber, B. Jordon-Thaden, C. Krantz, O. Novotný, S. Novotny, *et al.*, *Astrophys. J. Lett* **746**, L8 (2012).
4. D. M. Graninger, E. Herbst, K. I. Öberg, and A. I. Vasyunin, *Astrophys. J* **787**, 74 (2014), 1404.5338.
5. K. L. J. Rygl, A. Brunthaler, M. J. Reid, K. M. Menten, H. J. van Langevelde, and Y. Xu, *Astron. Astrophys* **511**, A2 (2010), 0910.0150.
6. M. Fich and L. Blitz, *Astrophys. J* **279**, 125 (1984).
7. K. L. J. Rygl, A. Brunthaler, A. Sanna, K. M. Menten, M. J. Reid, H. J. van Langevelde, M. Honma, K. J. E. Torstensson, and K. Fujisawa, *Astron. Astrophys* **539**, A79 (2012), 1111.7023.
8. M. Ott, A. Witzel, A. Quirrenbach, T. P. Krichbaum, K. J. Standke, C. J. Schalinski, and C. A. Hummel, *Astron. Astrophys* **284**, 331 (1994).
9. N. Schneider, T. Csengeri, S. Bontemps, F. Motte, R. Simon, P. Hennebelle, C. Federrath, and R. Klessen, *Astron. Astrophys* **520**, A49 (2010), 1003.4198.
10. J. Askne, B. Hoglund, A. Hjalmarson, and W. M. Irvine, *Astron. Astrophys* **130**, 311 (1984).
11. E. A. Bergin, P. F. Goldsmith, R. L. Snell, and H. Ungerechts, *Astrophys. J* **431**, 674 (1994).
12. O. L. Ryabukhina, M. S. Kirsanova, M. Wienen, and C. Henkel, *INASAN Science Reports* **5**, 207 (2020).
13. P. T. P. Ho and C. H. Townes, *Ann. Rev. Astron. Astrophys* **21**, 239 (1983).
14. M. Tafalla, P. C. Myers, P. Caselli, and C. M. Walmsley, *Astron. Astrophys* **416**, 191 (2004).
15. K. A. Marsh, A. P. Whitworth, and O. Lomax, *Mon. Not. R. Astron. Soc* **454**, 4282 (2015), 1509.08699.
16. K. A. Marsh, A. P. Whitworth, O. Lomax, S. E. Ragan, U. Becciani, L. Cambrésy, A. Di Giorgio, D. Eden, D. Elia, P. Kacsuk, *et al.*, *Mon. Not. R. Astron. Soc* **471**, 2730 (2017), 1707.03808.
17. R. Banerjee, R. E. Pudritz, and D. W. Anderson, *Mon. Not. R. Astron. Soc* **373**, 1091 (2006), astro-ph/0609428.
18. T. Liu, Y. Wu, and H. Zhang, *Astrophys. J. Lett* **775**, L2 (2013), 1306.0046.
19. F. F. S. van der Tak, J. H. Black, F. L. Schöier, D. J. Jansen, and E. F. van Dishoeck, *Astron. Astrophys* **468**, 627 (2007), 0704.0155.
20. T. Hirota, S. Yamamoto, H. Mikami, and M. Ohishi, *Astrophys. J* **503**, 717 (1998).

21. H. Beuther, F. Wyrowski, K. M. Menten, J. M. Winters, S. Suri, W. J. Kim, L. Bouscasse, C. Gieser, M. Sawczuck, I. B. Christensen, *et al.*, *Astron. Astrophys* **665**, A63 (2022), 2207.10964.
22. J. Di Francesco, D. Johnstone, H. Kirk, T. MacKenzie, and E. Ledwosinska, *Astrophys. J. Suppl. Ser* **175**, 277 (2008), 0801.2595.